Quantum dissipative dynamics of adsorbates near metal surfaces: A surrogate Hamiltonian theory applied to hydrogen on nickel

Roi Baer and Ronnie Kosloff
Department of Physical Chemistry and the Fritz Haber Research Center, The Hebrew University, Jerusalem 91904, Israel

(Received 26 September 1996; accepted 18 February 1997)

Dissipative dynamics of an adsorbate near a metal surface is formulated consistently by replacing the infinite system-bath Hamiltonian by a finite surrogate Hamiltonian. This finite representation is designed to generate the true short time dynamics of a primary system coupled to a bath. A detailed wave packet description is employed for the primary system while the bath is represented by an array of two-level systems. The number of bath modes determines the period the surrogate Hamiltonian reproduces the dynamics of the primary system. The convergence of this construction is studied for the dissipating Harmonic oscillator and the double-well tunneling problem. Converged results are obtained for a finite duration by a bath consisting of 4–11 modes. The formalism is extended to dissipation caused by electron-hole-pair excitations. The stopping power for a slow moving proton is studied showing deviations from the frictional limit at low velocities. Vibrational line shapes of hydrogen and deuterium on nickel were studied. In the bulk the line shape is mostly influenced by nonadiabatic effects. The interplay between two baths is studied for low temperature tunneling between two surface sites of hydrogen on nickel. A distinction between lattice modes that enhance the tunneling and ones that suppress it was found. © *1997 American Institute of Physics.* [S0021-9606(97)00720-4]

I. INTRODUCTION

The dynamics of molecules adsorbed on metal surfaces are complicated due to the simultaneous encounter with dissipative forces from two origins: electronic and phononic. Electronic dissipative forces are caused by the interaction of the free metal electrons, or more precisely from electron-hole pairs interacting with the adsorbate. These electron-hole pairs are able to exchange a continuous amount of energy. The other source of dissipative forces are the lattice vibrations or phonons which again form a band of energy levels. In this study, a consistent quantum theory is proposed to describe the short time dissipative dynamics of an adsorbate interacting with a metal surface. The formulation is cast into a wave packet and surrogate Hamiltonian description.

The basic idea is to distinguish between the dynamics of the primary system, the adsorbate, and that of the bulk which consists of the electronic and lattice degrees of freedom. The focus of the study is the dynamics of the primary system which therefore is described in detail. The treatment of the bulk, or the bath modes, includes the minimum details required to specify their influence on the primary system.

The idea of partitioning the system into primary and bath modes has been the key element in the quantum theory of dissipative dynamics. Starting from the work of Bloch,[1–3] reduced equations of motion for the primary system have been derived. The reduction is obtained by performing a partial trace over the bath degrees of freedom resulting in a Liouville description of the primary mode. The most well studied derivation is based on the assumption of weak coupling between the system and bath leading to a differential equation describing the systems dynamics.[4–7] In this derivation, commonly called Redfield dynamics, the influence of the bath is described by its correlation functions. This basic derivation has been supplemented by the requirement that the reduced equations of motion have the semi-group form, meaning that they preserve the complete positivity of the density operator.[8–10]

A complementary approach to dissipative dynamics is to axiomatically require a semigroup form. This leads to a general form for the reduced evolution equations.[11–13] These equations allow a consistent study of different dissipative models,[14,15] but require an empirical treatment when a particular system is studied. Such an approach has been used for modeling the photodesorption of NO from a nickel surface,[16–18] where the influence of the metal electrons was imposed empirically by using the semigroup form.

The practical disadvantage of both the semigroup and the Redfield theories is that they are formulated in Liouville space where the state of the system is represented by a density operator. This fact squares the number of required representation points in comparison to a wave function description. Although powerful numerical techniques have been developed to solve the dynamics in Liouville space[6,19–22] it still is extremely taxing to treat these problems, limiting the scope of systems that can be studied.

The approach presented in this paper is based on constructing a surrogate finite system bath Hamiltonian, which in the limit of an infinite number of bath modes generates the true systems dynamics. This is done by renormalizing the system-bath interaction term in the surrogate Hamiltonian. To reduce further the computational effort, the bath modes are represented by the elementary two-level system (TLS). The primary system is represented by the Fourier method,[23–25] allowing a very general description. The dynamics generated by the finite surrogate Hamiltonian are able to reproduce, for a specified period of time, the true system-bath dynamics. This construction is not Markovian and therefore differs from the Redfield or semigroup treatments. The use of a finite number of degrees of freedom to represent the bath limits the length of time in which the dynamics is consistent with that of an infinite bath. The finite nature of the bath usually shows up as recurrences which eventually appear. Increasing the number of bath modes postpones the recurrence to a later time, thus the number of modes needed is determined by the time scale of the dynamics.

The surrogate Hamiltonian approach is close in spirit to real time path integral techniques,[26,27] where a large many-body propagator is constructed and approximated. These approximations represent the bath modes as Harmonic oscillators,[28–31] for which the path integration can be carried out analytically.[32]

Other wave packet approaches to describe dissipative phenomena have been proposed. Significant effort has been devoted to mean field methods which approximate the many-body wave function in a product form. These methods known as TDSCF[33] or TDH[34] neglect explicit correlation. They form the base for quantum-classical methods[35–39] where the primary part is treated quantum mechanically and the bath classically or semi-classically.[40,41] TDSCF and variants which take into consideration some correlation have been applied extensively to atomic sticking on cold surfaces[42–46] Their primary drawback is that they contain uncontrollable approximations. The mean field method can be corrected by explicitly including correlations. The most sophisticated method is the multi-configuration time dependent Hartree (MC-TDH).[47,48] When applied to a system-bath encounter it has the same flavor as the surrogate Hamiltonian method.

Another dissipative wave packet method equivalent to the semigroup approach has been developed by Percival and others.[49–53] The method constructs a non-linear stochastic Schrödinger equation, which is solved using Monte Carlo techniques. It has the advantage of generality, but has numerical difficulties including slow convergence. This approach is simple to understand by considering a quantum system influenced by a time dependent stochastic potential. The evolution can be followed either by averaging the evolution operator[54] or by following individual realization of the stochastic force and averaging all the realizations at the end.

The surrogate Hamiltonian method is applied to a variety of dynamical dissipative processes taking place on metals. Vibrational spectral linewidths are a direct measure of dissipative forces. In the linear response limit the line shape is the Fourier transform of the dipole–dipole correlation function. Decay of correlation due to dissipative forces is reflected by the linewidth. The interplay between the nonadiabatic and phononic effects on vibrational line shapes[55,56] has been the subject of numerous theoretical studies. For high frequency modes, most of the effect is due to electron-hole-pair excitations. Electronic effects have been studied using density functional[57,58] or molecular orbital[59,60] theories. For lower vibrational frequencies, comparable to the Debye cutoff frequency, the phonons make a significant contribution to the line shape. A fingerprint of this contribution is the strong temperature dependence.[56]

The stopping power by metal electrons[61–63] of a fast moving ion is another case in which dissipative forces are responsible. For kinetic energies above the Fermi energy of the electrons the dissipative forces are purely frictional. At low kinetic energies, the surrogate Hamiltonian method shows that the dissipative effect is different.

Dissipative forces play a dominant role in tunneling. The reason being that tunneling is exponentially sensitive to all variables which influence the dynamics. An extreme case is that dissipative forces can stop tunneling completely.[64–67] Tunneling through a barrier of a double-well potential is used in this study as a benchmark to validate the surrogate Hamiltonian theory. The theory is then applied to low temperature diffusion of hydrogen on a nickel surface. Both phononic and electronic dissipative forces on the primary tunneling system are to be considered.

II. GENERAL FRAMEWORK

The dynamics under study is staged in the multimode coupled system-bath entity. The surrogate Hamiltonian method presented in this section is designed to study the dynamics of a finite system coupled to an infinite multimode bath at low temperature. It is assumed that the bath has a continuous infinity of modes each of which is coupled only infinitesimally to the finite system under study. This means that at low temperatures the bath is well approximated as a collection of independent harmonic oscillators, even when the overall coupling of the system to the bath is strong. An additional assumption is that the coupling to each mode is linear in the mode's displacement. This assumption is always well justified when the overall bath-system coupling is sufficiently weak, but it may also be applicable for strong coupling.

The complex bath and its coupling to the system have to be reduced to a tractable computational scheme. The first task is to construct a representation of the coupled system which can be systematically improved enabling a study of convergence characteristics. Once the representative wave function has been constructed, dynamics is determined based on the expansion of the evolution operator $\hat{\mathbf{U}}(t)=\exp(-i\hat{\mathbf{H}}t/\hbar)$ or the Green operator $\hat{\mathbf{G}}(E)=(E-\hat{\mathbf{H}})^{-1}$ in terms of a Chebychev polynomial series.[23,24] The propagation enables a direct extraction of observable information.

A. Representation of the coupled system

The system-bath representation is developed through the study of the total Hamiltonian. This Hamiltonian is partitioned into the primary system's bare Hamiltonian $\hat{\mathbf{H}}_{\mathbf{s}}$ the bath Hamiltonian $\hat{\mathbf{H}}_{\mathbf{B}}$ and an interaction term $\hat{\mathbf{H}}_{\mathbf{int}}$ leading to:

$$\hat{\mathbf{H}}=\hat{\mathbf{H}}_{\mathbf{s}}+\hat{\mathbf{H}}_{\mathbf{B}}+\hat{\mathbf{H}}_{\mathbf{int}}. \tag{2.1}$$

The primary system Hamiltonian has the form:

$$\hat{\mathbf{H}}_{\mathbf{s}} = \hat{\mathbf{T}} + V_s(\hat{\mathbf{R}}), \tag{2.2}$$

where $\hat{\mathbf{T}} = \hat{\mathbf{P}}^2/2M$ is the kinetic energy of the primary system and V_s is an external potential which is a function of the system coordinates $\hat{\mathbf{R}}$. The bath Hamiltonian $\hat{\mathbf{H}}_{\mathbf{B}}$ is decomposed to an infinite sum of normal modes:

$$\hat{\mathbf{H}}_{\mathbf{B}} = \sum_j \epsilon_j \hat{\mathbf{b}}_{\mathbf{j}}^{\dagger} \hat{\mathbf{b}}_{\mathbf{j}}. \tag{2.3}$$

The index j is a multidimensional index describing a complex bath of Bosonic modes with energies ϵ_j. Finally, the interaction term is a multiplication of a dimensionless geometric function $f(\hat{\mathbf{R}})$ with a Boson mode $\hat{\mathbf{b}}_{\mathbf{j}}^{\dagger}$ of potential coupling strength V_j:

$$\hat{\mathbf{H}}_{\mathbf{int}} = f(\hat{\mathbf{R}}) \sum_j V_j (\hat{\mathbf{b}}_{\mathbf{j}}^{\dagger} + \hat{\mathbf{b}}_{\mathbf{j}}). \tag{2.4}$$

The operators $\hat{\mathbf{b}}_{\mathbf{j}}^{\dagger}$ and $\hat{\mathbf{b}}_{\mathbf{j}}$ are Boson type creation and annihilation operators, obeying the commutation rules:

$$[\hat{\mathbf{b}}_{\mathbf{j}}, \hat{\mathbf{b}}^{\dagger}{}_{j'}] = \delta_{j,j'} \hat{\mathbf{1}}. \tag{2.5}$$

This system-bath Hamiltonian already represents a drastic reduction in complexity compared to the generic system-bath entity, mainly due to the simple linear (in the bath coordinate) interaction term. Nevertheless, for the specific system under study where an adsorbate interacts with the electronic and phonon baths, it will be shown that this description is reasonable.

Equations (2.1)–(2.4) serve as the starting point of the investigation, but further reduction is required since these equations are too involved to be treated directly. The problem is simplified by observing that the bath modes are uninteresting by themselves. Only their influence on the primary system has to be considered. The goal is to assemble a Hamiltonian consisting of a finite number of bath modes, which faithfully represents the dynamics of the primary system under the influence of an infinite bath for a finite time. This means that a systematic approach to converge a specific dynamical question has to be developed.

Such a goal is achieved by transforming the physically rich Boson bath to a simplified finite bath. This is done by examining the Heisenberg equations of motion for the primary system:

$$\begin{aligned} \dot{\hat{\mathbf{R}}} &= \hat{\mathbf{P}}/M, \\ \dot{\hat{\mathbf{P}}} &= -\nabla V_s(\hat{\mathbf{R}}) - \nabla f(\hat{\mathbf{R}}) \left(\sum_j V_j \hat{\mathbf{b}}_{\mathbf{j}}^{\dagger} + H.C. \right). \end{aligned} \tag{2.6}$$

The bath enters these equations through the operator:

$$\sum_j V_j \hat{\mathbf{b}}_{\mathbf{j}}^{\dagger} + H.C. = \int \sqrt{J(\epsilon)} \hat{\mathbf{B}}^{\dagger}(\epsilon) d\epsilon + H.C., \tag{2.7}$$

where a creation operator $\hat{\mathbf{B}}^{\dagger}(\epsilon)$ for an *interaction-Boson* is defined:

$$\hat{\mathbf{B}}^{\dagger}(\epsilon) = \frac{1}{\sqrt{J(\epsilon)}} \sum_j V_j \hat{\mathbf{b}}_{\mathbf{j}}^{\dagger} \delta(\epsilon - \epsilon_j). \tag{2.8}$$

Similar equations exist for the corresponding annihilation operators. $J(\epsilon)$ in these equations are normalizing factors defined by:

$$J(\epsilon) = \sum_j |V_j|^2 \delta(\epsilon_j - \epsilon). \tag{2.9}$$

This definition ensures that $\hat{\mathbf{B}}_{\epsilon}^{\dagger}$ and $\hat{\mathbf{B}}_{\epsilon}$ retain the Boson commutation relations:

$$[\hat{\mathbf{B}}_{\epsilon}, \hat{\mathbf{B}}_{\epsilon'}^{\dagger}] = \delta(\epsilon - \epsilon'). \tag{2.10}$$

The Heisenberg equations of motion for the new Boson operators are obtained from the Hamiltonian of Eq. (2.1) by commutation:

$$\begin{aligned} \dot{\hat{\mathbf{B}}}(\epsilon) = -i\epsilon \hat{\mathbf{B}}(\epsilon) - i f(\hat{\mathbf{R}}) \sqrt{J(\epsilon)} \dot{\hat{\mathbf{R}}} = \hat{\mathbf{P}}/M, \ \dot{\hat{\mathbf{P}}} = -\nabla V_s(\hat{\mathbf{R}}) \\ -\nabla f(\hat{\mathbf{R}}) \int \sqrt{J(\epsilon)} \hat{\mathbf{B}}^{\dagger}(\epsilon) d\epsilon + H.C. \end{aligned} \tag{2.11}$$

The Hamiltonian which contains the dynamical information of these equations of motion is the surrogate Hamiltonian:

$$\begin{aligned} \hat{\mathbf{H}}_{\mathrm{surr}} = \hat{\mathbf{T}} + V_s(\hat{\mathbf{R}}) + \int \epsilon \hat{\mathbf{B}}^{\dagger}(\epsilon) \hat{\mathbf{B}}(\epsilon) d\epsilon \\ + f(\hat{\mathbf{R}}) \int \sqrt{J(\epsilon)} \hat{\mathbf{B}}^{\dagger}(\epsilon) d\epsilon + H.C. \end{aligned} \tag{2.12}$$

Formally, this Hamiltonian governs the dynamics of the primary $\hat{R} - \hat{P}$ system in a completely equivalent manner to the full Hamiltonian. This statement must be qualified since not all initial states of the bath exist in the Hilbert space of the surrogate Hamiltonian. However, since a Boltzmann average over the initial states is intended, this poses no practical problems. The consequence is that the system-bath is fully characterized by the normalizing function, often called the spectral density $J(\epsilon)$. A derivation using path integral methods leads to the same conclusion.[64]

The existence of the spectral density points the way to a convergent method of sampling the bath by a finite number of modes. The finite bath of N oscillators is constructed by requiring a spectral density which resembles, and, in the limit $N \rightarrow \infty$, converges to, the given spectral density of the full bath. The algorithm of sampling the Boson bath assumes the given spectral density function $J(\epsilon)$ is of finite support, so that there exists an interval of energies $[\epsilon_o, \epsilon_c]$ outside of which the density is zero. The interval is sampled by selecting N energy points: $\epsilon_0 < \epsilon_1 < \cdots < \epsilon_{N-1}$. For each energy Boson creation $\hat{\mathbf{B}}_m^{\dagger}$ and annihilation $\hat{\mathbf{B}}_m$ operators are defined. The energy sampling specifies a density of states for the discrete bath $\rho(\epsilon_m) \approx (\epsilon_{m+1} - \epsilon_m)^{-1}$. In conjunction with the spectral density, the density of states imposed by the sampling determines an effective interaction through the relation:

$$U_m \hat{\mathbf{B}}_m^\dagger \rho(\epsilon_m) = \sqrt{J(\epsilon_m)}\,\hat{\mathbf{B}}_m^\dagger(\epsilon_m). \tag{2.13}$$

Thus, for the discrete surrogate Hamiltonian, the strength of interaction between the mth Boson and the primary system is given by:

$$U_m = \sqrt{J(\epsilon_m)/\rho(\epsilon_m)}. \tag{2.14}$$

The discrete surrogate Hamiltonian therefore takes the following form:

$$\hat{\mathbf{H}} = \hat{\mathbf{T}} + V_s(\hat{\mathbf{R}}) + \sum_{m=0}^{N-1} \epsilon_m \hat{\mathbf{B}}_{\mathbf{m}}^\dagger \hat{\mathbf{B}}_{\mathbf{m}} + f(\hat{\mathbf{R}}) \sum_{m=0}^{N-1} U_m \hat{\mathbf{B}}_{\mathbf{m}}^\dagger + H.C. \tag{2.15}$$

This construction has the merit that as N increases and the sampling refined, the dynamical observables converge. The convergence progresses in time with increasing number of bath modes and is inversely proportional to the largest energy sampling interval $\rho(\epsilon_{\max})$. Although the Hamiltonian Eq. (2.13) describing the correlated system-bath dynamics is greatly simplified it is still untractable in a computational scheme except in a one or two mode approximation. In order to be able to check convergence a further reduction is required.

B. A Boson bath as a set of TLSs

Further reduction is based on the assumption is that the bath temperature is low. Under these conditions no single mode oscillator is highly excited. This allows each bath mode to be represented by a two-level system (TLS), leading to a replacement of the Boson operators by TLS operators:

$$\hat{\mathbf{b}}^\dagger \rightarrow \hat{\sigma}_+ ,$$

$$\hat{\mathbf{b}} \rightarrow \hat{\sigma}_- . \tag{2.16}$$

Notice that the commutation relations also transform:

$$[\hat{\mathbf{b}}, \hat{\mathbf{b}}^\dagger] = 1 \rightarrow [\hat{\sigma}_-, \hat{\sigma}_+] = 1 - 2\hat{\mathbf{n}}, \tag{2.17}$$

where $\hat{\mathbf{n}} = \hat{\mathbf{b}}^\dagger \hat{\mathbf{b}} \rightarrow \hat{\mathbf{n}} = \hat{\sigma}_+ \hat{\sigma}_-$. Since $\langle \hat{\mathbf{n}} \rangle$ is 1 for an excited TLS and 0 otherwise, the violation of the commutation relations is small if none of the TLSs get highly excited. For higher bath temperatures a three level system formulation can be built along the same lines.

The numerical implementation of the dynamics of a subsystem coupled to N two-level systems (TLS) is best understood by first following the special case of a one mode $N=1$ bath. In this case the wave function is represented as a two-component spinor

$$\Psi(R) = \begin{pmatrix} \phi_0(R) \\ \phi_1(R) \end{pmatrix}. \tag{2.18}$$

The "0" component corresponds to spin down while the "1" component to spin up. The functions $\phi_m(R)$ are defined on equally spaced grids although other representation techniques are possible. The R-independent spin operators appearing in the Hamiltonian are represented as 2×2 matrices in the 2 component vector space:

$$\hat{\mathbf{b}}^\dagger = \begin{pmatrix} 0 & 0 \\ 1 & 0 \end{pmatrix}, \quad \hat{\mathbf{b}} = \begin{pmatrix} 0 & 1 \\ 0 & 0 \end{pmatrix}, \quad \hat{\mathbf{n}} = \hat{\mathbf{b}}^\dagger \hat{\mathbf{b}} = \begin{pmatrix} 0 & 0 \\ 0 & 1 \end{pmatrix}. \tag{2.19}$$

For the general N case, a wave function is represented as a spinor of 2^N components bit ordered. This means that the mth component represents a spin arrangement determined by the 1's (spin up) and 0's (spin down) in it's binary representation. Each component $\phi_m(R)$ is defined on the equally spaced grid. The Fourier method[23,24] is used for the representation of the primary system operators.

The wave function representation is designed to efficiently perform sums of spin operators. The algorithm for applying the number operator for the kth spin, $\hat{\mathbf{n}}_{\mathbf{k}}$, on the wave function Ψ, consists of multiplying the component ϕ_m by the kth bit of the binary representation of the integer m (0 or 1).

Applying the operator $\Sigma_j V_j(R) \hat{\mathbf{b}}_{\mathbf{j}}^\dagger$ is performed by recursion. The recursion is based on the structure of the matrix representation of the interaction operator. Observing the matrix representation of the three mode case although this matrix is never actually computed or stored reveals the general pattern:

$$\mathscr{V}_3 = \begin{pmatrix} 0 & V_1 & V_2 & 0 & V_3 & 0 & 0 & 0 \\ V_1 & 0 & 0 & V_2 & 0 & V_3 & 0 & 0 \\ V_2 & 0 & 0 & V_1 & 0 & 0 & V_3 & 0 \\ 0 & V_2 & V_1 & 0 & 0 & 0 & 0 & V_3 \\ V_3 & 0 & 0 & 0 & 0 & V_1 & V_2 & 0 \\ 0 & V_3 & 0 & 0 & V_1 & 0 & 0 & V_2 \\ 0 & 0 & V_3 & 0 & V_2 & 0 & 0 & V_1 \\ 0 & 0 & 0 & V_3 & 0 & V_2 & V_1 & 0 \end{pmatrix}. \tag{2.20}$$

The general recursive form of the matrix is described as follows. The $2^N \times 2^N$ matrix $\mathscr{V}_N$ is defined by:

$$\mathscr{V}_N = \begin{pmatrix} \mathscr{V}_{N-1} & V_N \mathbf{1}_{N-1} \\ V_N^* \mathbf{1}_{N-1} & \mathscr{V}_{N-1} \end{pmatrix}. \tag{2.21}$$

The definition is recursive with $\mathbf{1}_m$ being the $2^m \times 2^m$ unit matrix and $\mathscr{V}_{N=0} = 0$. The operator $\mathscr{V}_N$ consists of only diagonal operations, reducing the numerical effort to a quasilinear one ($M \log M$), in the number of spinor components ($M = 2^N$).

This algorithm contains all possible system-bath correlations. It is possible to restrict the number of simultaneous bath excitations. The most extreme restriction includes only a single phonon excitation, yielding an algorithm resembling the model of Stiles *et al.*[68] for phonon dissipation in inelastic collisions with metal surfaces. Such models have also been used for calculating sticking probabilities.[69,44]

C. System-bath dynamics

The primary system is represented by the Fourier method,[23–25] enabling multidimensional systems to be analyzed with no restriction on the potential shape. The exponential convergence of the method allows an elimination of errors due to representation.

Extracting dynamical information on the system requires propagation of an initial wave function by applying the evolution operator:

$$\Psi(t)=\hat{\mathbf{U}}(t)\Psi(0)=e^{-i\hat{\mathbf{H}}t/\hbar}\Psi(0). \tag{2.22}$$

The time dependence of the expectation value of any operator is determined by:

$$\langle\hat{\mathbf{A}}(t)\rangle=\langle\Psi(t)|\hat{\mathbf{A}}|\Psi(t)\rangle. \tag{2.23}$$

Frequency domain observables can be extracted from the half Fourier transform of various correlation functions:

$$\begin{aligned}C(\omega)&=\hbar\int_0^\infty e^{i\omega t}\langle\Psi(0)|\chi(t)\rangle dt\\&=\langle\Psi(0)|\hat{\mathbf{G}}(\hbar\omega)\chi(0)\rangle,\end{aligned} \tag{2.24}$$

where $\hat{\mathbf{G}}(E)=(E-\hat{\mathbf{H}})^{-1}$ is the Green's operator.

A general, accurate, stable and efficient method of executing these calculations is to expand the evolution operator or the Green's function operator in a series of Chebychev polynomials $T_n(\hat{\mathbf{H}})$ where $\hat{\mathbf{H}}$ is the Hamiltonian operator linearly scaled and shifted so that it's spectrum is in the range $\{-1,1\}$.[24,23] The expansion coefficients are functions of t for the evolution operator $\hat{\mathbf{U}}(t)$ or of E for the Greenian operator $\hat{\mathbf{G}}(E)$. When the Hamiltonian is completely hermitian, the expansions are both accurate and extremely stable. When the Hamiltonian has a nonhermitian component, these expansions are still stable, provided a slightly different scaling is performed for the Hamiltonian (see Ref. 70 for details). An alternative is to use a Newtonian polynomial expansion.[71] These techniques will be used for all the dynamical calculations shown in this study.

The propagator technique is also used to construct the initial state for the calculation. Propagating in imaginary time leads eventually to the fully correlated groundstate of the combined system-bath entity.[72] By employing a filter-diagonalization method[73,74] other eigenstates are extracted directly. Thermal observables are obtained by Boltzmann weighting the results from the individual calculations.

III. APPLICATION TO MODEL PROBLEMS

The application of the surrogate Hamiltonian to well studied model problems exemplifies its ability to describe dissipative phenomena. An important aspect to be addressed is the convergence of the method with respect to the number of bath modes.

A. The harmonic oscillator in an Ohmic bath

A popular benchmark system for dissipative dynamics is the relaxing Harmonic oscillator. When an oscillator is immersed in a bath, its frequency will shift due to the interaction and energy relaxation and dephasing will take place. A simple model is the harmonic oscillator coupled linearly to a bath:

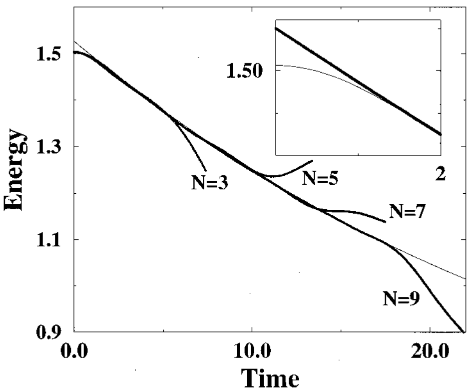

FIG. 1. The energy relaxation of the harmonic oscillator. The energy expectation value is shown for an increasing number of bath modes (3,5,7,9) for a zero temperature Ohmic bath with $\alpha=0.01$ and $\epsilon_3=3$. The thin line represents an exponential decay obtained from a semi-group weak coupling limit. The insert shows the short time dynamics which deviates from the semigroup result. (Note: 1 period of the oscillator is equal to 2π.)

$$\hat{\mathbf{H}}=\frac{\hat{\mathbf{P}}^2}{2}+\frac{\hat{\mathbf{R}}^2}{2}+\sum_j\epsilon_j\hat{\mathbf{b}}_j^\dagger\hat{\mathbf{b}}_j+\hat{\mathbf{R}}\sum_j V_j(\hat{\mathbf{b}}_j+\hat{\mathbf{b}}_j^\dagger). \tag{3.1}$$

The bath is described by a linear spectral density, $J(\epsilon)=\alpha\epsilon$ with a cutoff frequency of ϵ_c. This type of bath is known as an Ohmic bath.[75] The dimensionless parameter α determines the strength of the coupling. A finite bath with equally spaced sampling of the energy range was used. Other sampling strategies, such as the exponential sampling used in Section III B gave essentially similar results. The weak coupling limit predicts a pure exponential decay of energy which for zero temperature has the rate: $\Gamma=2\pi\alpha\omega_0$.[76]

The surrogate Hamiltonian is applied to a relaxing harmonic oscillator with a coupling parameter $\alpha=0.01$ and $\epsilon_c=3$. The calculation was performed with an increasing number of TLSs which progressively pushed the converged part of the approximation to longer times (Fig. 1). The period of convergence t_c, from Fig. 1 is inversely proportional to the sampling interval $t_c\approx2\pi\hbar/\rho_{\max}=2\pi\hbar N/\epsilon_c$ and linear with the number of bath modes N for equal sampling.

The dephasing phenomena of the oscillator is best observed through the study of the dipole correlation function:

$$C(t)=\frac{\langle\psi_g|\hat{\mathbf{R}}e^{-\frac{i}{\hbar}\hat{\mathbf{H}}t}\hat{\mathbf{R}}|\psi_g\rangle}{\langle\psi_g|\hat{\mathbf{R}}^2|\psi_g\rangle}. \tag{3.2}$$

The autocorrelation function is shown in Fig. 2 together with the weak coupling exponential envelope.

For this mode there is no pure dephasing. Therefore $T_1=\frac{1}{2}T_2$. This relation is confirmed by the calculation.

For the case of strong coupling, the bath parameters were $\alpha=0.3$ and $\epsilon_c=1.3$. The resulting energy and dipole auto correlation function as a function of time are shown in Fig. 3. The calculation was performed with an increasing number of TLSs. It is seen that energy is very quickly dissipated in the course of about half a period. The energy decays to a value of 0.6, higher than the oscillator 0.5 groundstate. The decay exhibits damped oscillations of the energy.

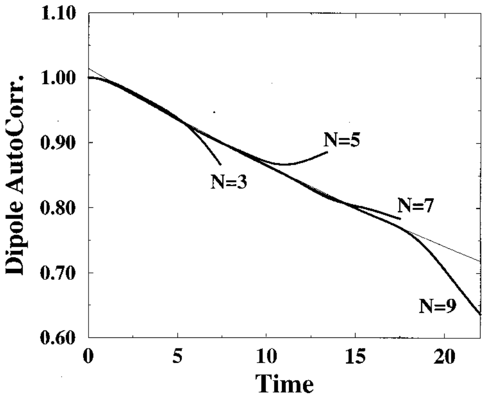

FIG. 2. The absolute value of the autocorrelation function of the dipole function for the relaxing Harmonic oscillator weakly coupled to the bath. The dynamics is shown with an increasing number of bath modes. The thin lines represent the weak coupling envelope.

The absolute part of the autocorrelation function is shown in Fig. 4. The strongly coupled case converges slowly at times longer than one period of the harmonic oscillator. The decay times, estimated from the converged part of the functions shows that for this system $T_1 \approx T_2$.

B. The effects of a Ohmic bath on double-well tunneling

Crossing a potential energy barrier is a cornerstone in chemical research. Kramers over 50 years ago[77,78] has pointed out the crucial role dissipative forces have on this process. The most problematic issue is the dissipative effects on tunneling dynamics and on the crossover from Arrhenius kinetics to groundstate tunneling.[67,66,79–81] A popular model system for this problem is the symmetric double-well potential and its low temperature analog, the dissipative two state system, often termed the spin-bose problem.[82] This model has been studied by using Feynman path integral approaches,[64,66] renormalization-group methods[83] and Redfield dynamics theory.[65]

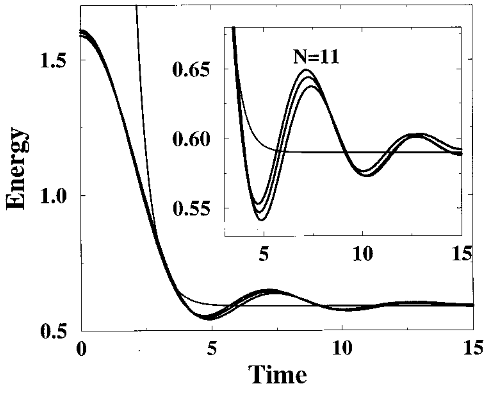

FIG. 3. The energy relaxation of the harmonic oscillator for strong coupling case. The energy expectation value is shown for an increasing number of bath modes (7,9,11) for a zero temperature linearly coupled Ohmic bath with $\alpha = 0.3$ and $\epsilon_c = 1.3$. The thin line represents an exponential decay obtained from a semi-group weak coupling limit. The insert shows the long time energy decay.

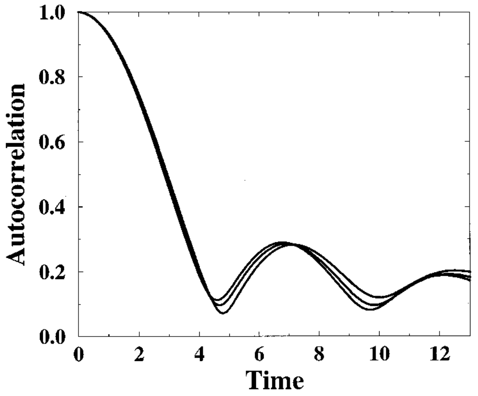

FIG. 4. The absolute value of the autocorrelation function of the dipole function for the relaxing harmonic oscillator strongly coupled to the bath. The dynamics is shown with an increasing number of bath modes.

The Hamiltonian for the symmetric double-well is:

$$\hat{\mathbf{H}} = \frac{\hat{\mathbf{P}}^2}{2M} + V_D(\hat{\mathbf{R}}) + \sum_j h_j(\hat{\mathbf{x}}_\mathbf{j}, \hat{\mathbf{p}}_\mathbf{j}) + \frac{\hat{\mathbf{R}}}{R_0} \sum_j C_j \hat{\mathbf{x}}_\mathbf{j}. \tag{3.3}$$

Here, M, $\hat{\mathbf{P}}$, $\hat{\mathbf{R}}$ are the mass, momentum and position of the double-well oscillator, V_D is the double-well potential with separation distance R_o, and h_j is the Hamiltonian of the jth harmonic oscillator, with frequency, mass, position and momentum: ω_j, m_j, $\hat{\mathbf{x}}_\mathbf{j}$ $\hat{\mathbf{p}}_\mathbf{j}$. The bath system coupling is characterized by the spectral density $J(\epsilon) = \Sigma_j |V_j|^2 \delta(\epsilon - \epsilon_j)$, where $V_j = C_j / \sqrt{2 m_j \omega_j}$.

Specifically the spin-bose system with an Ohmic bath is studied, characterized by a spectral density linear in energy: $J(\epsilon) = \alpha\epsilon$. It is known[75] that for $\alpha \approx 1$ the dissipation greatly influences the tunneling rate. Furthermore, a transition to a completely localized regime occurs at the critical coupling value of $\alpha_c = 1$.[83–85]

A numerical representation of the Ohmic bath, has to address the many energy scales of the problem. This fact is characteristic of Ohmic baths and is the reason why renormalization techniques are useful for this problem.[86] The bath sampling technique has to span different energy scales, resulting in an exponential sampling: $\epsilon_n = \epsilon_0 b^n$, $n = 0 \cdots N-1$ where ϵ_0 is the low energy cutoff and b is the sampling base. This scheme naturally introduces a high energy cutoff for the spectral density at $\epsilon_c = \epsilon_0 b^{N-1}$. It is known that the critical behavior at $\alpha = 1$ exists only when the high frequency cutoff is raised to infinity. For a finite cutoff frequency, the tunneling rate Δ behaves as $\Delta \approx \Delta_o (\epsilon_0 / \epsilon_c)^\alpha$, where Δ_o is the rate without dissipation.[83]

The double-well potential studied is described by potential:

$$\hat{\mathbf{V}}(R) = \tfrac{1}{2}\left(V_+ + V_- - \sqrt{(V_+ - V_-)^2 + 4C}\right), \tag{3.4}$$

where $V_\pm = 1/2k(R \pm R_o)^2$. The various parameters for the calculation are tabulated in Table I. For these parameters, a

TABLE I. Parameters of the double-well tunneling calculation.

Parameter	Value (a.u.)
Minima separation R_o	0.7
Spring constant k	0.029 38
Oscillator mass M	1836
Minima coupling C	0.001 00
Oscillator representation grid size	64 points
Oscillator grid spacing ΔR	0.1250
Low energy cutoff ω_0	1.328e-05
Number of bath spins N	8
Base for exponential sampling b	2
High energy cutoff $\omega_{N-1}=\omega_0 b^{N-1}$	1.700e-03

bath of 8 spins $(b=2)$ was sufficient to converge the dynamics up to a period of 1 psec. For longer times additional Bosons are required. The tunneling time of the bare double-well oscillator is of that order. The 8 Bosons imply using spinors of 256 wave packets, each represented by a 64 point grid, totaling a $\frac{1}{2}$ megabyte of memory for each wave function. The calculation times for each run were approximately 1–2 hours on a Silicon-Graphics R8000 machine.

The calculation is initialized by decoupling the two potential wells [setting $C=0$ in Eq. (3.4)]. The groundstate ψ_g of the left well is determined by propagating in imaginary time on a trial wave function:

$$e^{-\hat{\mathbf{H}}t}\psi_{\text{trial}} \overset{t\rightarrow\infty}{\longrightarrow} \psi_g . \tag{3.5}$$

With this initial state, the two wells are recouped and the full dynamics takes over: $\psi(t)=\exp(-i\hat{\mathbf{H}}t)\psi_g$. The mean position of the oscillator, $\langle\psi(t)|\hat{\mathbf{R}}|\psi(t)\rangle$, is the dynamical observable recorded during the evolution.

Figure 5 shows the mean position of the wave function as a function of time for various values of the dissipation parameter α. The exponential growth in the transition time is clearly shown in the figure. The oscillations under the influence of the dissipation appear damped and irregular.

The initial tunneling rate averaged over the first psec is shown, in logarithmic scale in Fig. 6. Also shown is the tunneling rate predicted by dimensional arguments,[86] which is merged with the calculation for $\alpha<1$.

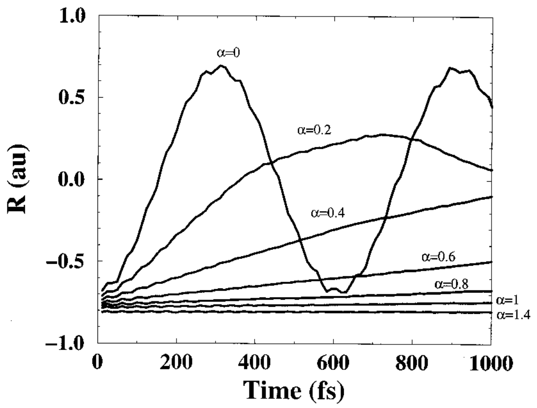

FIG. 5. The expectation value of the position R of a double-well oscillator for various values of the dissipation parameter sa. An eight TLS bath was required to converge the results, until a duration of $t=1000$ fsec.

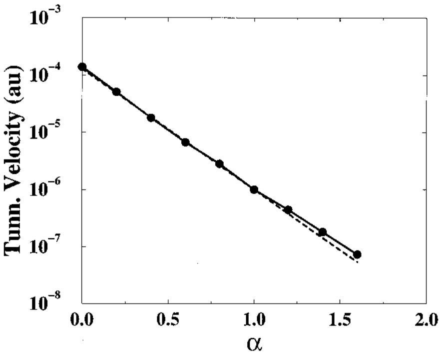

FIG. 6. The rate of tunneling, represented by the averaged velocity $d/dt\langle R\rangle$ as a function of the dissipation parameter α. The dashed line indicates the theoretical result $\Delta=\Delta_0(\omega_0/\omega_{N-1})^{\alpha}$.

The conclusion from the above benchmark systems is that the surrogate Hamiltonian implementation is able to capture quantitatively the dissipative dynamics associated with correlation functions and quantum tunneling dynamics. Once confidence has been gained, the method can be applied to more realistic encounters.

IV. NONADIABATIC EFFECTS ON ADSORBATES

The unique features of the interaction of the primary system with the electronic continuum requires a modified formulation. The adiabatic part of the interaction of the hydrogen with the semi-free metal electrons can be accounted for by employing density functional calculations[87–90] or related methods such as the empirical EAM.[91,92] The nonadiabatic interactions are responsible for the dissipative phenomena.[56,93]

In order to simulate the nonadiabatic phenomena they must be reduced to an effective heat-bath formulation. The basic idea is to construct the appropriate finite heat bath which models the interaction of an interstitial atom with the conduction electrons of the metal for a specified period of time. The relevant spectral density calculation is based on a screened Coulomb electron-proton interaction.

The nonadiabatic interaction model describes the system's dynamics by an Anderson type Hamiltonian, where the interaction of the proton with the conduction electrons is explicit:

$$\hat{\mathbf{H}} = \frac{\hat{\mathbf{P}}^2}{2M} + V(\hat{\mathbf{Z}}) + \sum_{\mathbf{k}} \epsilon_{\mathbf{k}}\hat{\mathbf{n}}_{\mathbf{k}} + \Omega^{-1}\sum_{\mathbf{k}\mathbf{k}'} V_{\mathbf{k}-\mathbf{k}'}e^{i(\mathbf{k}-\mathbf{k}')\cdot\hat{\mathbf{Z}}}\hat{\mathbf{a}}^{\dagger}_{\mathbf{k}}\hat{\mathbf{a}}_{\mathbf{k}'} . \tag{4.1}$$

Here $|\mathbf{k}\rangle$ represents the free one-electron states of the conduction band, characterized by 3 dimensional momentum $\mathbf{k}$ and energy $\epsilon_{\mathbf{k}}=\hbar^2k^2/2\mu_e$. The operators $\hat{\mathbf{a}}^{\dagger}_{\mathbf{k}}$ and $\hat{\mathbf{a}}_{\mathbf{k}}$ are the electron creation and annihilation operators for the state $|\mathbf{k}\rangle$. The number operator becomes: $\hat{\mathbf{n}}_{\mathbf{k}}=\hat{\mathbf{a}}^{\dagger}_{\mathbf{k}}\hat{\mathbf{a}}_{\mathbf{k}}$. The interaction term between the proton and the electrons is proportional to the inverse volume of the electron gas Ω. This is a manifestation of the locality of the proton-electron interaction potential $v(r)$ which has a finite range κ^{-1} where κ is the screening parameter. The constants $V_{\mathbf{k}-\mathbf{k}'}$ are the Fourier transform of the proton-electron interaction potential:

$$V_q = \int e^{i\mathbf{q}\cdot\mathbf{r}} v(r) d^3 r. \tag{4.2}$$

Following Muller–Hartman, Ramakrishnan and Toulouse (MHRT),[94,95] the Hamiltonian is reformulated to describe the coupling of the proton to a bath of Bosons. This approximation is valid for low temperatures when a local proton-electron gas interaction takes place as in the case of the proton dynamics problems considered here. Alternative forms of Bosonization are discussed in Ref. 86. The Bosonization is formulated in terms of electron-hole-pair excitations which are created and annihilated by the following operators:

$$\hat{\mathbf{b}}_{\mathbf{j}}^{\dagger} = \hat{\mathbf{a}}_{\mathbf{k}'}^{\dagger}\hat{\mathbf{a}}_{\mathbf{k}}; \quad \hat{\mathbf{b}}_{\mathbf{j}} = \hat{\mathbf{a}}_{\mathbf{k}}^{\dagger}\hat{\mathbf{a}}_{\mathbf{k}'} \quad \{|\mathbf{k}| < k_F, \quad |\mathbf{k}'| > k_F\}. \tag{4.3}$$

An electron-hole pair (EHP) is characterized by two single electron states designated by the six dimensional index $\mathbf{j} = (\mathbf{k}, \mathbf{k}')$ with $k < k_F$ and $k' > k_F$, where k_F is the Fermi momentum of the conduction electron gas. A $\mathbf{j}$ EHP represents an excitation energy $\epsilon_{\mathbf{j}} = \epsilon_{\mathbf{k}'} - \epsilon_{\mathbf{k}}$ and momentum $\mathbf{q}_{\mathbf{j}} = \mathbf{k}' - \mathbf{k}$. As long as the electron gas is close to its groundstate, these operators approximately obey the Boson commutation relations:

$$[\hat{\mathbf{b}}_{\mathbf{j}}, \hat{\mathbf{b}}_{\mathbf{j}'}^{\dagger}] = \delta_{\mathbf{j},\mathbf{j}'} \hat{\mathbf{1}}. \tag{4.4}$$

For a thorough discussion of this Bosonization see Ref. 94.

The Heisenberg equations of motion for the EHP operators $\hat{\mathbf{b}}_{\mathbf{j}}^{\dagger}$ and the proton operators $\hat{\mathbf{P}}$ ands $\hat{\mathbf{Z}}$ can be obtained from the Hamiltonian of Eq. (4.1). An inspection reveals that the following effective Hamiltonian generates the same dynamics:[94]

$$\hat{\mathbf{H}} = \frac{\hat{\mathbf{P}}^2}{2M} + V_o(\hat{\mathbf{Z}}) + \sum_{\mathbf{j}} \epsilon_{\mathbf{j}} \hat{\mathbf{n}}_{\mathbf{j}} + \Omega^{-1} \sum_{\mathbf{j}} [V_{\mathbf{q}_{\mathbf{j}}} e^{i\mathbf{q}_{\mathbf{j}}\cdot\hat{\mathbf{Z}}} \hat{\mathbf{b}}_{\mathbf{j}}^{\dagger} + H.C.]. \tag{4.5}$$

This Hamiltonian is simpler than the original Anderson type. It is similar to the Polaron Hamiltonian.[32] For a one dimensional proton it is shown in the Appendix that the EHP bath is uniquely and fully determined by the two parameter nonadiabatic spectral density:

$$J(\epsilon, q) = \frac{1}{\Omega^2} \sum_{\mathbf{j}} |V_{\mathbf{q}_{\mathbf{j}}}|^2 \delta(\epsilon_{\mathbf{j}} - \epsilon) \delta(q_{\mathbf{j}}^z - q). \tag{4.6}$$

This function, with a screened-Coulomb electron-proton interaction is calculated analytically using the Fermi–Dirac distribution at zero temperature. An analytical approximation for the nonadiabatic spectral density is (see the Appendix):

$$J(\epsilon, q) = \frac{\mu_e^2 e^2 \epsilon}{\pi^2 \hbar^4 \kappa^3} \left(\arctan\left(\frac{(2k_F - |q|)\kappa}{\kappa^2 + 2k_F|q|} \right) + \frac{2k_F|q|}{4k_F^2 + \kappa^2} - \frac{|q|\kappa}{q^2 + \kappa^2} \right), \tag{4.7}$$

where μ_e and e are the electron mass and charge respectively, κ is the inverse screening length and $\hbar k_F$ is the momentum of an electron at the Fermi level. The last two parameters are determined by the electron density (see the Appendix).

V. ELECTRONIC FRICTION FOR HYDROGEN DYNAMICS

When a proton moves in a uniform electron gas it dissipates its translational energy.[62] It is known that for velocities lower than the Fermi velocities of the electrons, the energy dissipation has the form of friction dependence:

$$\frac{dE_k}{dZ} = -\eta v_z, \tag{5.1}$$

where v_z is the velocity of the proton and E_k is its kinetic energy. The friction coefficient η is independent of the hydrogen mass and velocity. The theory of hydrogen translational energy dissipation in an electron gas has been developed and experimentally tested in the range of energies higher than the Fermi energy $E_k \gg \epsilon_F$ (usually $E_k \approx 1$ kev). Here, the models of nonadiabatic interactions presented in Section IV and the numerical treatment of these models in Section II B are used to explore the very low velocity regime, where the proton kinetic energy is much smaller than the Fermi energy.

The friction phenomena has been simulated using six TLSs which sample two q-values $\otimes$ three ϵ-values of the spectral density $J(q,\epsilon)$ representing the nonadiabatic bath. The first stage consists of localizing the atom by using a confining harmonic potential. The ground state of the combined EHP-proton system is then calculated by propagating in negative imaginary time. In the second stage the harmonic potential is replaced by a constant potential and the relaxed spinor wave packet is subjected to a *kick* executed by the momentum shift operator $e^{iP_o\hat{\mathbf{Z}}}$. The evolution operator is then applied to propagate the energetic wave packet coupled to the cold Fermion sea. During the evolution the expectation value of the proton kinetic energy is recorded at regular intervals. Figure 7 shows relaxation of the kinetic energy due to electronic friction.

The friction coefficients as a function of the electron density and different proton momenta are shown in Fig. 8. A cutoff energy $\epsilon_c = 0.27$ eV was used in the calculations. The high momentum cases converged to a velocity independent friction regime. The convergent value of the friction coefficient η fits well with calculations based on the Lindhard theory for screened-Coulomb interactions (see Ref. 62). The results are not particularly sensitive to the value of the cutoff

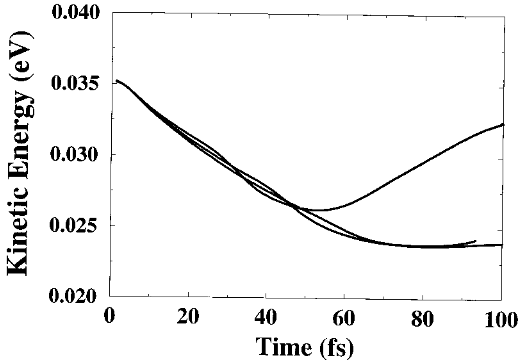

FIG. 7. The kinetic energy as a function of time of a slow proton moving in an electron gas. The electron density parameters is $r_s = 1.5$ and the cutoff energy is $\epsilon_c = 0.27$ eV. Three calculations are shown corresponding to different samplings of the EHP bath: 4, 6, and 8 TLSs.

energy and a cutoff energy of $\epsilon_f = 1$ eV has yielded similar results. For low velocities the friction becomes velocity dependent.

Another feature seen in Fig. 8 is that the friction coefficients diminish as the electron density is lowered. This occurs *in spite of the increase* in the spectral density. Since the spectral density is a Fermi-golden rule expression for energy rate dissipation, it is obvious that the relevant dynamics are more complex than a low order perturbation description. The energy dissipation is less efficient for a low density gas, due to the fact that the Fermi momentum $\hbar k_F$ decreases. This leads to a less efficient coupling of the proton motion because of the long wavelength associated with the interaction in Eq. (4.5).

VI. LINE SHAPES OF HYDROGEN IN NICKEL

The chemistry of hydrogen embedded in nickel has been recently probed on a molecular level.[96,97] Using HREELS spectroscopy the vibrational line of bulk hydrogen was identified. The line shape gives insight to the dissipative forces acting on the hydrogen atom. Such forces influence significantly the dynamics of bulk hydrogen, in particular the resurfacing motion.[98] Using the EAM scheme[91,92] the hydrogen/nickel potential energy surface has been calculated together with the local electron density. These results serve as input for calculating the nonadiabatic line broadening of hydrogen in an interstitial subsurface site and in a surface adsorption site.

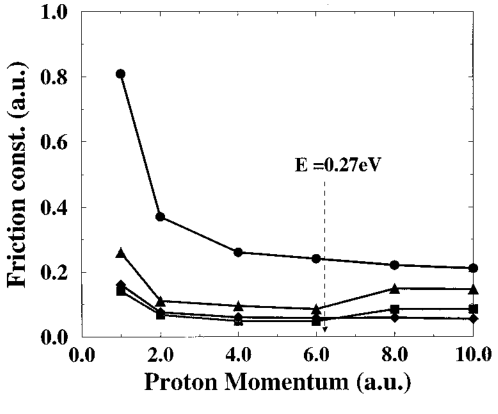

FIG. 8. The friction coefficient for a proton moving in an electron gas as a function of the translational momentum and of the electron density: $r_s = 1.5$—circles, $r_s = 2$—triangles, $r_s = 3$—squares and $r_s = 4$—diamonds. The cutoff energy for these calculations was $\epsilon_f = 0.27$ eV.

Vibrational adiabatic line broadening of atomic hydrogen on metal surfaces has been calculated by Persson and Hellsing[57,58] yielding values of 10–30 cm^{-1} (FWHM) depending on electron density. It has been estimated that phonon contributions are small for high frequencies.[56]

A. Line shape of hydrogen in bulk nickel

The phonon bath contribution to the line shape at low temperature has been calculated by the surrogate Hamiltonian method and found to be extremely small. This is a result of the vibrational misfit between the slow lattice phonons (cutoff frequency at $\approx 300\ \mathrm{cm}^{-1}$) and the hydrogen bulk frequency (970 cm^{-1} for the mode perpendicular to the surface). The nonadiabatic effect was calculated using the method of Section IV with the primary system potential taken as an EAM adiabatic potential.

Details of the procedure for estimating the decay times are as follows. First, the ground state ψ_g and ground energy E_g of the total system is determined by evolving a trial function in imaginary time. Then, the ground state is operated on by the position operator of the oscillator. This yields the state $\psi(0) = \hat{\mathbf{R}}\psi_g$. The state $\psi(0)$ is now propagated in time using the full Hamiltonian. During the evolution the oscillator energy $E(t) = \langle \psi(t) | H_{\mathrm{osc}} | \psi(t) \rangle$ and dipole correlation $C(t) = e^{iE_g t/\hbar} \langle \psi(0) | \psi(t) \rangle$ are monitored. Their decay rates determine T_1 and T_2.

The EHP bath sampling was refined until convergence of the slopes was obtained, to within 6%. This was done by considering several baths. The first bath consisted of 4 (2e⊗2q) EHP's. Then, additional calculations were made with 6 (3e⊗2q) and then 8 (4e⊗2q) EHP baths, where it was found that the results were much the same as the 4 EHP bath. This means that an extensive energy sampling is not required. Next, a refinement of the q-sampling was tried. A bath of 8 (2e⊗4q) EHP's was used and the slopes were increased by more than 25%. Finally a 12 (2e⊗6q) EHP bath was run, and the slopes changed by less than 6%, signaling that sufficient sampling was obtained. The calculational effort grows exponentially with the number of EHP modes. Thus it is quite difficult to obtain better converged results. The 12 EHP bath converges the dynamics for one period of the oscillator before recurrences set in. This time was sufficient to observe an energy absorption of nearly 10% of the excitation.

The nonadiabatic line broadening and decay times are shown in Table II as a function of the interstitial electron density. In interstitial nickel the electron density parameter $r_s \approx$ 2.1 yields a line width of $\approx 23\ \mathrm{cm}^{-1}$ (FWHM). Linewidth of hydrogen on W(100) and Mo(100) been measured[99] by IR spectroscopy yeilding a line width in the range of 12 to 65 cm^{-1}. The large isotope effect measured leads to the

TABLE II. Vibrational relaxation times of bulk hydrogen.

r_s	T_1 [fsec]	T_2 [fsec]	Γ (FWHM) cm^{-1}
1.5	170	220	50
2.	330	460	23
3.	622	634	17

nonadiabatic relaxation mechanism. The monotonic relation between linewidth and electron density allows use of the vibrational line shape of hydrogen as a direct measure of local electron density.

B. Line shape of hydrogen on a Ni(100)

Hydrogen resides as an atomic species on a nickel (100) surface with typical frequencies of 588 cm^{-1} for the perpendicular mode and 387 cm^{-1} for the transverse mode.[100]

Since the transverse mode has vibrational frequencies similar to the phonon frequencies, an attempt to calculate the line broadening is made. The surface phonon bath is approximated as an Ohmic bath, $J(\epsilon)=\alpha\epsilon$ with a cutoff frequency set at $\omega_c=300\ \text{cm}^{-1}$.[101] The interaction of the vibrating atom with the bath is chosen as $V = \hat{\mathbf{R}}/\mathbf{a_o}\Sigma_\mathbf{j}\mathbf{V_j}(\hat{\mathbf{b}}_\mathbf{j}^\dagger + \hat{\mathbf{b}}_\mathbf{j})$, R being the coordinate of the vibrating atom and a_o is the Bohr radius. In this form, the dimensionless constant α is approximately equal to unity.[101] The bath was represented by an increasing number of modes equally sampling the energy range. Nine modes were sufficient to converge the dynamics for a period of 150 fs. No significant energy and dipole correlation damping were observed for this time period. Similar results were found for the deuterium isotope.

The electronic line broadening for this vibrational mode was also calculated, using the method of the previous section. The nonadiabatic dissipation was calculated using the electron density at a hydrogen adsorption site, of $r_s=2.5$. The bath was represented by equally sampling four q values and three energy values of the spectral density in Eq. (4.7). The nonadiabatic vibrational line broadening contribution for hydrogen was 20 cm^{-1} (FWHM). The heavier, slowly moving deuterium is less affected with a spectral linewidth of 8 cm^{-1} (FWHM).

VII. DISSIPATION AND SURFACE DIFFUSION

Low temperature surface diffusion of hydrogen is dominated by tunneling. This is confirmed by experimental results of Gomer,[102] showing a temperature independent diffusion regime below temperatures of 100 °K Tunneling calculation of hydrogen on Ni(100) have been performed by Wonchoba and Truhlar,[81] however dissipation effects were not taken into account in that work, although phonon assisted tunneling was. Wahnstrom *et al.*[101] have recently investigated the same system employing a path integral method to incorporate the influence of phonon collisions. Both of these calculations show a temperature independent diffusion regime with a crossover temperature, 65 K in Ref 81 and 40 K in Ref. 101. More recent measurements performed by Zhu,[103] show a crossover temperature of 160 K. Quantitatively, the calculated tunneling rates and the crossover temperatures are much lower than the experimental values. The inclusion of phonon interactions by Wahnstrom hindered the tunneling leading to even larger discrepancy between theory and experiment.

The model employed by Wahnstrom assumed that the bath was approximately Ohmic. The bath parameters were determined from a molecular dynamics calculation of the surface motion. The calculated diffusion rates for this model are 8 orders of magnitude lower than the measured diffusion rates. This result reflects the fact that an Ohmic bath with $\alpha\approx 1$ suppressed the tunneling rates (see Section III B). The discrepancy can be explained by noticing that other types of phonon motion can enhance the tunneling, through the effect of lowering the tunneling barriers (phonon assisted diffusion[104]). To investigate the two competing trends a calculation based on the surrogate Hamiltonian theory was initiated.

Four separate calculations of the tunneling rates were carried out based on the same adiabatic potential adopted from Wonchoba *et al.*[81] The first calculation was performed with a frozen lattice establishing a benchmark. The second calculation employed an Ohmic bath linearly coupled to the tunneling motion (see Eq(3.3)). The parameters of the bath were taken from Ref. 101. In the third calculation the primary motion was coupled to an Ohmic bath by a Gaussian coupling function: $f(R)=\exp(-(R-R_b)^2/2\sigma^2)$ in Eq. (2.4). R_b was positioned at the barrier peak and σ was small enough to localize the coupling function to the immediate vicinity of barrier. The dynamics induced by any mode in the bath in this case raises and lowers the barrier relative to the stationary well minima. This is in contrast to the linearly coupled Ohmic bath where for each mode, the barrier is stationary and the two potential wells oscillate out of phase. Finally, the simultaneous effects of the two types of baths was investigated. The spectral density of each of these baths is not known, so only a qualitative analysis is possible. To assist the comparison the two baths were chosen to have the same Ohmic dependence and cutoff frequencies.

The calculation was initiated by determining the eigenstates of the adsorption site. The tunneling route was artificially blocked and imaginary time propagation was employed in conjunction with the filter-diagonalization method of Neuhauser.[73] For the frozen lattice five initial states were calculated where the highest eigenvalue was close to the top of the barrier. When baths are added the number of initial eigenstates grows significantly.

Once these states are available the tunneling route is opened and a negative imaginary potential is placed in the empty site. This potential regularizes the problem allowing to operate on the initial wavefunction with the Green operator $G(E)=(E-H)^{-1}$.[70] This operation filters out the tunneling state with energy close to E.[74] A few calculations required a repeated applications of $G(E)$ in order to filter out the pure tunneling state. The imaginary part of this state's energy is directly related to the tunneling rate. The flux of the tunneling state is another measure of the tunneling rate.

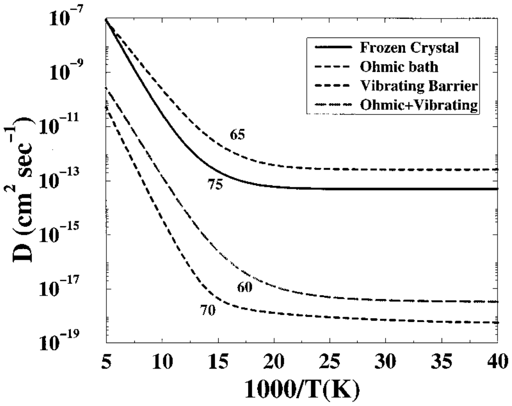

FIG. 9. Diffusion rates for hydrogen on Ni(100) as a function of inverse temperature. The solid line is a frozen crystal calculation with a crossover temperature of 75 °K. The lowest diffusion rate is that of the linearly coupled Ohmic bath with a crossover at 67 °K. Next, the highest diffusion rates correspond to a Gaussian coupling to a Ohmic bath, simulating independent barrier breathing mode, with a crossover at 65 °K. Finally, the results of integration between the 2 Ohmic baths is given by the long-dashed line. The measured diffusion constant at the temperature independent regime is 2×10^{-12} (Ref. 102) and 10^{-11} (Ref. 103). In the double bath calculation each bath was sampled by 3 modes (TLSs).

An agreement between these two values is a direct indication of convergence.

The calculated thermal diffusion rates are shown in Fig. 9. It is seen that the linearly coupled Ohmic bath destroys the groundstate tunneling motion, suppressing it by five orders of magnitude compared to the frozen lattice tunneling rates. This result is consistent with the calculations of Wahnstrom.[101] Contrarily, the fluctuating barrier model was found to promote the tunneling by a factor of 5. The combined motion, where both baths are given equal strength exhibits higher tunneling rates than the linear bath alone. For low temperature this enhancement is a by a factor of 10. These results are still way below the frozen lattice calculations and the experimental observations.

The nonadiabatic effect on the tunneling was calculated using the method presented in Section IV. It was found to have a relatively weak suppressing effect on the tunneling rate and crossover temperatures compared to the effects of the phonons. This is due to the small coupling between the hydrogen and the conduction electrons at the surface.

As a conclusion, to explain the low temperature, tunneling rates the coupling function between the phonon baths and the hydrogen atom. This has been recently done for the resurfacing of hydrogen in nickel, where MD simulations were used to calculate the spectral density, revealing that approximately three baths are required to describe the phonon effects (see Ref. 98 for an example of a detailed analysis). It is also probable that the adiabatic potential energy surface employed overestimates the tunneling barrier.

VIII. DISCUSSION

The elucidation of dynamical encounters in condensed phases has to include dissipation. The surrogate Hamiltonian approach presented in this study incorporates dissipative dynamics without compromising on the quantum nature of the processes involved. A sufficient number of bath modes represented as two-level-systems are employed to describe the dissipative dynamics for a specified observable. The converged period t_c depends on the number of bath modes through the maximum discrete density of states $\rho(e_{\max})$. For an equal sampling of the energy range t_c is linear with the number of modes. These considerations are a manifestation of the time-energy uncertainty principle where for short time dynamics a course grained representation of the energy is sufficient. The present study is consistent with the observation of Cederbaum *et al.*[48] that incorporating more independent bath modes is more important than a detailed description of a single mode.

For a particular system-bath construction the combined system is a single entity. The use of the Chebychev propagation methods[25] leads to a uniform convergence in all the sampled energy band. This approach differs from other treatments of dissipative dynamics in which there is an operative distinction between the representation of the primary system and the bath. This distinction is obvious for the quantum/classical methods or the Liouville space method in which the bath is not considered explicitly at all.

In the present approach the description of the primary system is unrestricted. A harmonic or unharmonic or double-well potential can all be represented by the same grid. The use of a grid also permits an unrestricted system-bath coupling function.

The time propagation requires an initial state. This is done in two steps: The first is to locate the energy eigenfunctions of the combined system-bath starting from below. The procedure used is based on propagation in imaginary time. The number of eigenfunctions required grows with temperature and exponentially with the number of bath modes. The eigenfunctions found incorporate naturally the shift in the primary systems frequencies due the interactions with the bath.

Once these stationary states are found a perturbation is applied to the system, designed to mimic an experimental setup. For example, in the calculation of stopping power a momentum shift operator is imposed on the system, instantly creating a moving particle. For simulating weak field absorption spectrum the dipole operator is applied to the initial state and the relaxation in time of the dipole correlation functions is then transformed to the line shape function. This formalism caters naturally to simulations of ultrafast experiment where a short electromagnetic pulse is applied to the system and the induced polarization is followed by a weak probe. Simulations of thermal processes requires to repeat the propagation step for each initial state and then to Boltzmann average the results. The need for averaging an the exponential increase with the number of modes practically limits the treatment to low temperatures.

The present procedure should be compared to methods based in Liouville space.[6,19–22] For the relaxing Harmonic oscillator a sufficient Liouville description would require a density operator represented by a matrix of size 64×64. The surrogate Hamiltonian method with a wavepacket of dimensions 64×2^n with $n=6$ TLS bath modes has an equal representation size. Unlike the Liouville dynamics the wave packet calculation has to be repeated many times to describe a thermal encounter.

The two methods are not equivalent, the Liouville approach has the advantage that it can be constructed to lead asymptotically to the thermal equilibrium state. The surrogate Hamiltonian method which is not Markovian is able to describe the correct short time dynamics. For larger grid representations at low temperature the balance shifts toward the surrogate Hamiltonian approach. The surrogate Hamiltonian method avoids the complicated issue of calculating the relaxation tensor required in the Redfield or weak coupling theory.[20,105] This is of particular importance for simulating strong field ultrafast processes where the relaxation tensor has to be adjusted to include the effect of the external field.[106] The uniform structure of surrogate Hamiltonian method will naturally incorporate these effects.

The surrogate Hamiltonian approach can be extended to describe dissipative phenomena generated simultaneously by more than one bath. A natural example is vibrational line shapes of an adsorbate on metals where both electronic and phononic baths participate. For high frequency vibrational modes the line shape is dominated by nonadiabatic effects.

Tunneling dynamics is extremely sensitive to the dissipative environment. Different local modes can either enhance or suppress the tunneling dynamics. In the surrogate Hamiltonian each of these effects is represented by a separate bath. The spectral density of these different baths can be determined by analyzing the motion for several positions of the hydrogen atom on its adiabatic potential surface using MD simulations. In Ref. 98 an example of such a calculation has been worked out for the tunneling of subsurface hydrogen to a surface site in nickel. The detailed analysis has determined three operative baths. Tunneling dynamics is found to be extremely sensitive to the correlated motion of all these baths. This is a general conclusion for any tunneling motion influenced by its environment.

This study shows that the surrogate Hamiltonian theory leads to new insight into the dynamics of dissipating systems. More effort and comparative studies are still required to determine the range of utility and applicability of this new method.

ACKNOWLEDGMENTS

We thank Yehuda Zeiri for his help and numerous discussions. This research was partially supported by the Israel Science Foundation. The Fritz Haber Research Center is supported by the Minerva Gesellschaft für die Forschung, GmbH München, FRG.

APPENDIX: SPECTRAL DENSITY FOR A PROTON IN AN ELECTRON GAS

The starting point is the Hamiltonian of Eq. (4.5) describing a particle with coordinate Z in a potential well V_s, interacting with a bath of electron-hole-pairs (EHP). These Bosons are taken as the elementary excitations of a homogeneous noninteracting electron gas, of density $\rho_e^{-1}=(4\pi/3(r_s a_o)^3)$, where a_o is the Bohr radius and r_s is the electron packing parameter. Many-body effects such as screening are taken phenomenologically into account by modifying the electron-proton Coulomb interaction:

$$v(r)=-\frac{e}{r}\exp(-\kappa r), \tag{A1}$$

where e is the electron charge, $\kappa\approx 3\alpha/a_o\sqrt{r_s}$ is the inverse screening length and $\alpha=(4/9\pi)^{1/3}$.[62] Under this interaction, the electron hole pair coupling to the proton in Eq. (4.5) becomes:

$$V_{\mathbf{q}}=-\frac{4\pi e}{q^2+\kappa^2}. \tag{A2}$$

As shown for the phonon bath, the spectral density is extracted for the nonadiabatic interaction. The derivation is along the same lines as for the phonon case but different in details. Focus is on the proton dynamics, with the operators evolving according to the Heisenberg equations of motion:

$$\dot{\hat{\mathbf{Z}}}=\hat{\mathbf{P}}/M,$$

$$\dot{\hat{\mathbf{P}}}=-\frac{\partial}{\partial Z}V_o-i\Omega^{-1}\sum_{\mathbf{j}} V_{\mathbf{q_j}}q_{\mathbf{j}}^z e^{iq_{\mathbf{j}}^z\hat{\mathbf{Z}}}\hat{\mathbf{b}}_{\mathbf{j}}^\dagger+H.C. \tag{A3}$$

The harmonic bath enters the proton equations of motion through the operator $\Omega^{-1}\Sigma\mathbf{j}V_{\mathbf{q_j}}q_{\mathbf{j}}^z e^{iq_{\mathbf{j}}^z Z}\hat{\mathbf{b}}_{\mathbf{j}}^\dagger+H.C.$ In order to take this into account, a new Boson creation operator is defined:

$$\hat{\mathbf{B}}^\dagger(q,\epsilon)=\Omega^{-1}\frac{1}{\sqrt{J(q,\epsilon)}}\sum_{\mathbf{j}} V_{\mathbf{q_j}}\hat{\mathbf{b}}_{\mathbf{j}}^\dagger\delta(q_{\mathbf{j}}^z-q)\,\delta(\epsilon_{\mathbf{j}}-\epsilon), \tag{A4}$$

where $J(q,\epsilon)=\Omega^{-2}\Sigma_{\mathbf{j}}|V_{\mathbf{q_j}}|^2\delta(q_{\mathbf{j}}^z-q)\,\delta(\epsilon_{\mathbf{j}}-\epsilon)$ is the 2 dimensional spectral density. The $\hat{\mathbf{B}}(q,\epsilon)$ have the following Bosonic commutation relations:

$$[\hat{\mathbf{B}}(q,\epsilon),\hat{\mathbf{B}}(q',\epsilon')^\dagger]=\delta(q-q')\,\delta(\epsilon-\epsilon'). \tag{A5}$$

Equations of motion can be directly inferred from the Hamiltonian Eq. (4.5) leading to:

$$\dot{\hat{\mathbf{B}}}(q,\epsilon)=-i\epsilon\hat{\mathbf{B}}(q,\epsilon)+i\sqrt{J(q,\epsilon)}e^{iq\hat{\mathbf{Z}}}. \tag{A6}$$

The following Hamiltonian, which yields exactly the above Heisenberg equations can replace the more elaborate Hamiltonian given above:

$$\hat{\mathbf{H}}=\frac{\hat{\mathbf{P}}^2}{2M}+V_o(\hat{\mathbf{Z}})+\int \epsilon\hat{\mathbf{B}}(q,\epsilon)^\dagger\hat{\mathbf{B}}(q,\epsilon)dqd\epsilon$$

$$+\int [e^{iq\hat{\mathbf{Z}}}\sqrt{J(q,\epsilon)}\hat{\mathbf{B}}(q,\epsilon)^\dagger+H.C.]dqd\epsilon. \tag{A7}$$

The only relevant characteristic of the bath is the spectral density $J(q,\epsilon)$, dependent on two parameters. The spectral density can be calculated for the screened-Coulomb interaction. First, a calculation of the density of EHPs is made. Using the Fermi–Dirac distribution at $T=0$ $n_{\mathbf{k}}=\theta(k_F^2-\mathbf{k}^2)$

where $\theta(x)$ is the Heavyside function and k_F is the Fermi wave number of the electron gas, the EHP density is:

$$N(\mathbf{q}\epsilon)=\sum_{\mathbf{k}}\sum_{\mathbf{k}'} n_{\mathbf{k}}(1-n_{\mathbf{k}'})\,\delta(\epsilon-(\epsilon_{k'}-\epsilon_k))\,\delta(\mathbf{q}-(\mathbf{k}'-\mathbf{k})),$$
$$=\frac{\Omega^2\mu_e^2}{16\pi^5\hbar^4 q}\min\left(\epsilon;\epsilon_F-\frac{(\epsilon-\epsilon_q)^2}{4\epsilon_q}\right), \tag{A8}$$

where ϵ_F is the Fermi energy of the electron gas and $\epsilon_q \equiv \hbar^2 q^2/2\mu_e$. For the small excitations expected in the system, this density of excitations can be well approximated by the function:

$$N(\mathbf{q},\epsilon)\approx\frac{\Omega^2\mu_e^2\epsilon}{16\pi^5\hbar^4 q}\,\theta(2k_F-q). \tag{A9}$$

Using this approximation the spectral density becomes:

$$J(q,\epsilon)=\Omega^{-2}\int d^3q'\int d\epsilon' N(q,\epsilon)\left(\frac{4\pi e}{q'^2+\kappa^2}\right)^2$$
$$\times\,\delta(q-q_z')\,\delta(\epsilon-\epsilon'). \tag{A10}$$

A direct integration yields Eq. (4.7) in the text.

[1] F. Bloch, Phys. Rev. **70**, 460 (1946).
[2] F. Bloch, Phys. Rev. **102**, 104 (1956).
[3] F. Bloch, Phys. Rev. **105**, 1206 (1957).
[4] A. G. Redfield, Phys. Rev. **98**, 1787 (1955).
[5] A. G. Redfield, IBM J **1**, 19 (1957).
[6] W. T. Pollard and R. A. Friesner, Adv. Chem. Phys. **93**, 77 (1996).
[7] S. A Egorov and J. L. Skinner, J. Chem. Phys. **105**, 7047 (1996).
[8] E. B. Davies, Commun. Math. Phys. **39**, 91 (1974).
[9] E. B. Davis, *Quantum Theory of Open Systems* (Academic, New York, 1976).
[10] N. Van Kampen, *Stochastic Processes in Physics and Chemistry* (North-Holland, 1992).
[11] G. Lindblad, Commun. Math. Phys. **48**, 119 (1976).
[12] V. Gorini, A. Kossokowski, and E. C. G. Sudarshan, J. Math. Phys. **17**, 821 (1976).
[13] R. Alicki, K. Lendi, *Quantum Dynamical Semigroups and Applications* (Springer-Verlag, Berlin, 1987).
[14] S. Rice and R. Kosloff, J. Chem. Phys. **86**, 2153 (1982).
[15] R. Kosloff and M. A. Ratner, J. Chem. Phys. **77**, 2841 (1982).
[16] P. Saalfrank, R. Baer and R. Kosloff, Chem. Phys. Lett. **230**, 463 (1994).
[17] P. Saalfrank and R. Kosloff, J. Chem. Phys. **105**, 2441 (1996).
[18] O. Kühn and V. May, Chem. Phys. **208**, 117 (1996).
[19] M. Berman, R. Kosloff, and H. Tal-Ezer J. Phys. A **25**, 1283 (1992).
[20] W. T. Pollard and R. A. Friesner, J. Chem. Phys. **100**, 5054 (1994).
[21] O. Kühn and V. May, Chem. Phys. Lett. **225**, 511 (1994).
[22] G. Ashkenazi, U. Banin, A. Bartana, R. Kosloff, and S. Ruhman, Adv. Chem. Phys. **100** (1997).
[23] R. Kosloff, J. Phys. Chem. **92**, 2087 (1988).
[24] R. Kosloff, ''The Fourier Method,'' in *Numerical Grid Methods and Their Application to Schrodinger's Equation*, edited by C. Cerjan (Kluwer Academic, The Netherlands, 1993), p. 175.
[25] R. Kosloff, Annu. Rev. Phys. Chem. **45**, 145 (1994).
[26] K. Allinger, B. Karmeli, and D. Chandler, J. Chem. Phys. **84**, 1774 (1989).
[27] K. Allinger and M. A. Ratner, Phys. Rev. A **139**, 864 (1989).
[28] D. E. Makarov and N. Makri, Phys. Rev. A **48**, 3626 (1993).
[29] N. Makri and D. E. Makarov, J. Chem. Phys. **102**, 4600 (1995).
[30] F. Grossmann, J. Chem. Phys. **103**, 3696 (1995).
[31] G. A. Voth, Adv. Chem. Phys. **93**, 135 (1996).
[32] R. P. Feynman, (W. A. Benjamin, Inc., 1972).
[33] A. B. McCoy, R. B. Gerber, and A. Garcia-Vela, Annu. Rev. Phys. Chem. **45**, 275 (1994).
[34] M. Ehara, H.-D. Meyer, and L. S. Cederbaum, J. Chem. Phys. **105**, 8865 (1996).
[35] V. Buch, R. B. Gerber, and M. A. Ratner, J. Chem. Phys. **77**, 3022 (1982).
[36] R. B. Gerber and M. A. Ratner, Adv. Chem. Phys. **70**, 97 (1988).
[37] R. Kosloff and C. Cerjan, J. Chem. Phys. **81**, 3722 (1984).
[38] R. Alimi, R. B. Gerber, A. Dell Hammerich, R. Kosloff, and M. Ratner, J. Chem. Phys. **93**, 6484 (1990).
[39] E. R. Bittner and P. Rossky, J. Chem. Phys. **103** (1995).
[40] S. Mukamel, Annu. Rev. Phys. Chem. **41**, 647 (1990).
[41] L. E. Fried and S. Mukamel, Adv. Chem. Phys. **84**, 435 (1993).
[42] R. Kosloff and C. Cerjan, J. Chem. Phys. **81**, 3722 (1984).
[43] C. Cerjan and R. Kosloff, Phys. Rev. B **34**, 3832 (1986).
[44] B. Jackson, Comput. Phys. Commun. **80**, 119 (1994).
[45] N. E. Henriksen, G. D. Billing and F. Y. Hansen J. Phys. Chem. **96**, 223 (1992).
[46] E. R. Bittner and J. C. Light, J. Chem. Phys. **102**, 2614 (1995).
[47] R. Kosloff and A. D. Hammerich, Faraday Discuss. Chem. Soc. **91**, 239 (1991).
[48] G. A. Worth, H-D. Meyer, and L. S. Cederbaum, J. Chem. Phys. **105**, 4412 (1996).
[49] N. Gisin and I. C. Percival, J. Phys. A: Math. Gen. **25**, 5677 (1992).
[50] R. Dum, P. Zoller, and H. Ritch, Phys. Rev. A **45**, 4879 (1992).
[51] Y. Castin, J. Dalibard, and K. Molmer, Phys. Rev. Lett. **68**, 580 (1992).
[52] Y. Castin, K. Molmer, and J. Dalibard, J. Opt. Soc. Am. **10**, 524 (1993).
[53] J. Steinbach, B. M. Garraway, and P. L. Knight, Phys. Rev. A **51**, 3302 (1995).
[54] R. Kosloff, Physica **110A**, 346 (1982).
[55] R. Rydberg, ''Infrared spectroscopy of molecules adsorbed on metal surfaces,'' in *Advances in Chemical Physics*, edited by Lawley (Academic, New York, 1989), p. 498.
[56] D. C. Langreth and M. Persson, ''Vibrational relaxation and dephasing of molecules adsorbed on metal surfaces,'' in *Laser Spectroscopy and Photochemistry on Metal Surfaces*, edited by H.-L. Dai and W. Ho (World Scientific, Singapore, 1995), p. 498.
[57] M. Persson and B. Hellsing, Phys. Rev. Lett. **49**, 662 (1982).
[58] B. Hellsing and M. Persson, Phys. Script. **29**, 360 (1984).
[59] M. Head-Gordon and J. C. Tully, J. Chem. Phys. **96**, 3939 (1992).
[60] J. C. Tully, M. Gomez, and M. Head-Gordon, J. Chem. Phys. **96**, 3939 (1992).
[61] E. Fermi and E. Teller, Phys. Rev. **72**, 399 (1947).
[62] T. L. Ferrell and R. H. Ritchie, Phys. Rev. B **16**, 115 (1977).
[63] M. J. Puska and R. M. Nieminen, Phys. Rev. B **27**, 6121 (1983).
[64] A. J. Leggett, S. Chakravarty, A. T. Dorsey, M. P. A. Fisher, A. Garg, and W. Zwerger, Rev. Mod. Phys. **59**, 1 (1987).
[65] R. Silbey and R. A. Harris, J. Phys. Chem. **93**, 7062 (1989).
[66] H. Grabert, P. Olchowski, and U. Weiss, ''Quantum decay of dissipative systems,'' in *Path Summation: Achievements and Goals*, edited by Schulman *et al.* (World Scientific, Singapore, 1988), p. 227.
[67] V. A. Benderskii, D. E. Makarov, and C. A. Wight, Adv. Chem. Phys. **58**, 1 (1994).
[68] M. D. Stiles, J. W. Wilkins, and M. Persson, Phys. Rev. B **34**, 4490 (1986).
[69] B. Jackson, J. Phys. Chem. **97**, 6792 (1992).
[70] Y. Huang, D. J. Kouri, and D. J. Hoffman, J. Chem. Phys. **101**, 10 493 (1994).
[71] G. Ashkenazi, R. Kosloff, S. Ruhman, and H. Tal-Ezer, J. Chem. Phys. **103**, 10 005 (1995).
[72] R. Kosloff and H. Tal-Ezer, Chem. Phys. Lett. **127**, 223 (1986).
[73] M. R. Wall and D. Neuhauser, J. Chem. Phys. **102**, 8011 (1995).
[74] R. Baer, Y. Zeiri, and R. Kosloff, Phys. Rev. B, **54**, (1996).
[75] A. O Caldeira and A. J. Leggett, Physica A **121**, 587 (1983).
[76] W. H. Louisell, *Quantum Statistical Properties of Radiation* (Wiley, New York, 1990).
[77] H. A. Kramers, Physica **7**, 284 (1940).
[78] P. Talkner, P. Hanggi, and M. Borkovec, Rev. Mod. Phys. **62**, 251 (1990).
[79] B. Whaley, A. Nitzan and R. B. Gerber, ''Low temperature atom diffusion on surfaces: tunneling and energy band structure,'' in *Tunneling*, edited by J. Jortner and B. Pullman (D. Reidel, The Netherlands, 1986), p. 297.
[80] A. Auerbach, K. F. Freed, and R. Gomer, ''Tunneling in Surface Diffusion,'' in *Tunneling*, edited by J. Jortner and B. Pullman (D. Reidel, The Netherlands, 1986), p. 281.
[81] S. E. Wonchoba, W. P. Hu, and D. G. Truhlar, Phys. Rev. B **51**, 9985 (1995).
[82] A. O. Caldeira and A. J. Leggett, Phys. Rev. Lett. **46**, 211 (1981).
[83] V. Hakim, A. Muramatsu, and F. Guinea, Phys. Rev. B **30**, 464 (1984).

[84] A. J. Bray and M. A. Moore, Phys. Rev. Lett. **49**, 1546 (1982).
[85] S. Chakravarty, Phys. Rev. Lett. **49**, 681 (1982).
[86] F. Guinea, V. Hakim, and A. Muramatsu, Phys. Rev. B **32**, 4410 (1985).
[87] W. Kohn and L. J. Sham, Phys. Rev. A **140**, 1133 (1965).
[88] R. Car and M. Parrinello, Phys. Rev. Lett. **55**, 2471 (1985).
[89] R. G. Parr and W. Yang, *Density-Functional Theory of Atoms and Molecules* (Oxford University Press, New York, 1989).
[90] F. Besenbacher and J. K. Norskov, Prog. Surf. Sci. **44**, 5 (1993).
[91] M. S. Daw and M. I. Baskes, Phys. Rev. B **29**, 6443 (1984).
[92] T. N. Truony, D. G. Truhlar, and B. C. Garrett, J. Phys. Chem. **93**, 8227 (1989).
[93] N. E. Henriksen, G. D. Billing, and F. Y. Hansen, Surf. Sci. **227**, 224 (1990).
[94] T. V. Ramakrishnan, E. Muller-Hartmann, and G. Toulouse, Phys. Rev. B **3**, 1102 (1971).
[95] T. V. Ramakrishnan, E. Muller-Hartmann, and G. Toulouse, Solid State Commun. **9**, 99 (1971).
[96] A. D. Johnson, K. J. Maynard, S. P. Daley, Q. Y. Yang, and S. T. Ceyer, Phys. Rev. Lett. **67**, 927 (1991).
[97] Al. Utz, A. D. Johnson, S. P. Daley, and S. T. Ceyer, Science **257**, 223 (1992).
[98] R. Baer, Y. Zeiri, and R. Kosloff, Phys. Rev. B (to be published).
[99] Y. J. Chabal and A. J. Sievers, Surf. Sci. Rep. **44**, 211 (1988).
[100] A.-S Martensson, C. Nyberg, and S. Andersson, Surf. Sci. **205**, 12 (1988).
[101] T. R. Mattsson and G. Wahnstrom, Phys. Rev. B **51**, 1885 (1995).
[102] T-S. Lin and R. Gomer, Surf. Sci. **255**, 41 (1991).
[103] X. D. Zhu, A. Lee, A. Wong, and U. Linke, Phys. Rev. Lett. **68**, 1992 (1992).
[104] T. N. Truong and D. G. Truhlar, J. Phys. Chem. **91**, 6229 (1987).
[105] J. L. Skinner, B. B Laird, and L. Root, J. Lumin. **45**, 6 (1990).
[106] E. Geva, R. Kosloff, and J. L. Skinner, J. Chem. Phys. **102**, 8541 (1995).